

# Dimensional crossover of the integer quantum Hall plateau transition and disordered topological pumping

Matteo Ippoliti<sup>1</sup> and R. N. Bhatt<sup>2</sup>

<sup>1</sup>*Department of Physics and* <sup>2</sup>*Department of Electrical Engineering,  
Princeton University, Princeton NJ 08544, USA*

We study the quantum Hall plateau transition on rectangular tori. As the aspect ratio of the torus is increased, the two-dimensional critical behavior, characterized by a subthermodynamic number of topological states in a vanishing energy window around a critical energy, changes drastically. In the thin-torus limit, the entire spectrum is Anderson-localized; however, an *extensive* number of states retain a Chern number  $C \neq 0$ . We resolve this apparent paradox by mapping the thin-torus quantum Hall system onto a disordered Thouless pump, where the Chern number corresponds to the winding number of an electron's path in real space during a pump cycle. We then characterize quantitatively the crossover between the one- and two-dimensional regimes for large but finite aspect ratio, where the average Thouless conductance also shows anomalous scaling.

*Introduction.* The integer quantum Hall plateau transition [1] has a long and rich history as an example of the interplay between disorder and topology. While the quantization is ultimately due to the presence of a topological invariant [2, 3], its astonishing precision is due to disorder-induced localization of electron states away from the critical energy [4]. In a high magnetic field, the motion of electrons can be projected to the lowest Landau level (LLL). The LLL carries a non-zero *Chern number*, a topological invariant related to the Hall conductance, which forbids complete localization of the spectrum. A critical energy exists where the electron localization length  $\xi$  diverges, explaining the plateau transition as a quantum critical point that has successfully been studied by means of scaling theories [5]. However, the precise value of  $\nu$ , the critical exponent characterizing the divergence of  $\xi$ , and whether or not it agrees with experiment [6–8] (with implications for the relevance of interactions [9]), remains controversial [10–12].

Most numerical studies of the critical exponent have relied on strip geometries, using the transfer matrix approach for either the original continuum LLL problem [13, 14] or the Chalker-Coddington network model [15–18]. On the other hand, purely two-dimensional methods to determine  $\nu$  have been developed based on the topological character of individual eigenstates [19, 20] (an idea that has since been used in several studies [11, 21–27]), the disorder-averaged Hall [28, 29], Thouless [29, 30] and longitudinal [31] conductance, as well as quantum diffusion [32]. Here one considers a square torus geometry and both sides are scaled concurrently,  $L_x = L_y \sim N_\phi^{1/2}$  ( $N_\phi$  is the number of magnetic flux quanta through the system, proportional to the system's area). The number of states with nonzero Chern number (hereafter simply called Chern states) is found to diverge subextensively with system size, as  $N_\phi^{1-\frac{1}{2\nu}}$  [19]. The success of methods based on the Chern number in square geometry motivates studying the same physics in rectangular geometries  $L_x > L_y$  with varying as-

pect ratio  $a = L_x/L_y$ , and particularly in the quasi-one-dimensional limit  $a \rightarrow \infty$  at fixed thickness, reminiscent of the transfer matrix calculations. This is especially interesting because the defining feature of the 2D problem (the presence of a topologically robust Hall conductance, encoded in the Chern number  $C$ ) does not have an obvious one-dimensional counterpart. While the mathematical definition of  $C$  holds regardless of system size or aspect ratio, on physical grounds the system in the quasi-1D limit must be described by a local, disordered fermionic chain – essentially the Anderson model. The question then arises of what is the fate of Chern states under 1D scaling, and how the topological character of the LLL manifests once the system is mapped onto a 1D Anderson insulator.

One may reasonably expect, given the stronger tendency towards localization in one dimensional systems, that quasi-1D scaling will lead to a faster decay in the fraction of Chern states relative to the 2D case (where the fraction falls off as  $N_\phi^{-\frac{1}{2\nu}}$ ), perhaps even to saturate the lower bound  $N_\phi^{-1}$  (achieved if all states but one have  $C = 0$ ). In fact, we find quite the opposite: Chern states do *not* vanish under 1D scaling. On the contrary, they represent a *finite* fraction of all states – and we argue they asymptotically take over the *entire* spectrum!

As a byproduct, we also obtain the (longitudinal) Thouless conductance  $g$  [33]. Both the typical and average  $g$  decay exponentially with  $L_x$ , as is expected for localized one-dimensional systems. Interestingly though we find that the *average*  $g$  retains a memory of the 2D critical scaling.

Existing studies of one-dimensional scaling of the integer quantum Hall problem [34, 35] focus open boundary conditions, where the crossover is seen through mixing of topological edge states on opposite edges of the strip. Our edge-free torus geometry offers a different perspective on the problem and reveals fascinating and unexpected behavior – including the aforementioned proliferation of Chern states. Guided by these surprising nu-

merical findings, we develop a theoretical understanding based on a mapping to a disordered Thouless pump [36], and uncover the invariant corresponding to the 1D limit of the Chern number. A quantitative description of the proliferation of Chern states follows naturally from this perspective.

*Model and numerical method.* We consider a continuum model of two-dimensional (2D) electrons in a high perpendicular magnetic field such that the dynamics can be projected onto the LLL. The model is set on a rectangular torus with sides  $L_x, L_y$  such that  $L_x L_y = 2\pi N_\phi \ell_B^2$ , where  $\ell_B = \sqrt{eB/\hbar}$  is the magnetic length, which we set to 1 henceforth. We define the aspect ratio  $a = L_x/L_y$  and take  $a \geq 1$ . Disorder in the system is modeled by a Gaussian white noise potential. The torus has generalized periodic boundary conditions with angles  $\theta_{x,y}$ . These also represent magnetic fluxes through the two nontrivial loops in the torus and are needed to define and compute Chern numbers of individual eigenstates in the disordered problem. For each disorder realization, we compute and diagonalize the single-particle Hamiltonian on a lattice of boundary angles  $\theta$  and store the eigenvalues  $\{E_n(\theta)\}$  and eigenvectors  $\{|\psi_n(\theta)\rangle\}$ . The energies are used to calculate the Thouless conductance  $g_n \equiv \mathbb{E}_{\theta_y}[\sigma_{\theta_x} E_n(\theta)]$  ( $\mathbb{E}$  denotes averaging,  $\sigma$  denotes standard deviation), a measure of sensitivity to boundary conditions in the *long* direction; the wavefunctions are used to compute each eigenstate's Chern number  $C_n$  via a standard numerical technique [37]. Further details on the model and the numerical method are provided in the Supplemental Material [38].

*Density of Chern states.* With the method outlined above, we calculate the density of states with Chern number  $C$ ,  $\{\rho_C(E) : C \in \mathbb{Z}\}$ . These obey  $\sum_C \rho_C = \rho$  (total density of states) as well as  $\sum_C C \rho_C = \partial_E \sigma_{xy}$  (Hall conductance). Past studies [11, 19] have characterized the 2D critical behavior by looking at the density of “current-carrying states”,  $\rho_{\text{top}}(E) \equiv \rho(E) - \rho_0(E)$ . The width of  $\rho_{\text{top}}$  scales as  $N_\phi^{-1/2\nu_{2D}}$  in the 2D thermodynamic limit.

In the present context, we observe completely different behavior. Namely, the width of  $\rho_{\text{top}}$  does *not* vanish as  $L_x$  is increased. It stays roughly constant for  $a \gtrsim 1$ , and eventually starts *increasing* for  $a \gg 1$  (Fig. 1). This increase is due both to the broadening of  $\rho_{\pm 1}(E)$  (i.e. more pairs of Chern  $\pm 1$  states appearing away from the band center), and to an increase in higher- $|C|$  states. Despite these effects, the Hall conductance remains unchanged, and is determined by the shortest side of the torus [38].

This extensive number of topological “current-carrying states” seems to be incompatible with the localized nature of the spectrum (which we verify independently by means of the Thouless conductance). Reconciling these facts requires a careful analysis of the fate of Chern numbers as the dimensionality is tuned from  $d = 2$  to  $d = 1$  by increasing the aspect ratio  $a$ .

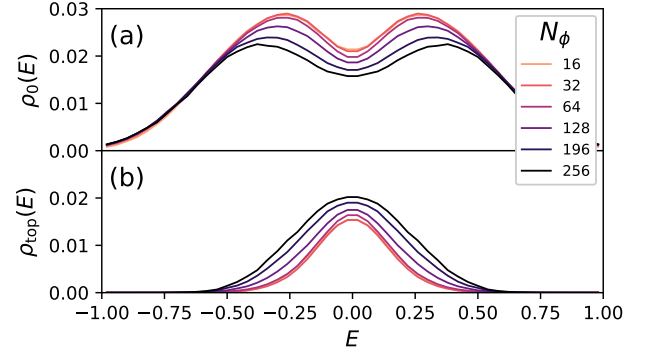


FIG. 1. Density of (a)  $C = 0$  and (b)  $C \neq 0$  states for fixed  $L_y = 10\ell_B$  and increasing  $N_\phi$ . The density of Chern  $C \neq 0$  states  $\rho_{\text{top}}(E)$  grows and broadens at the expense of  $\rho_0(E)$ .

*Thin-torus limit.* The above question is best addressed in the thin-torus limit  $L_y \ll \ell_B$ , though (as we shall clarify later) the answer we find also applies to finite  $L_y$ , provided  $a$  is sufficiently large. The LLL Hamiltonian in the thin-torus limit is approximated by the following local 1D fermionic chain,

$$H_{1D} = \sum_n v_n c_n^\dagger c_n + (t_n c_{n+1}^\dagger c_n + h.c.), \quad (1)$$

with  $v_n = V_0(x_n)$ ,  $t_n = e^{i\theta_x/L_x} V_1(x_n)$ , and  $x_n = (2\pi n + \theta_y)/L_y$ . The  $V_m$  are Fourier transforms of the LLL-projected real-space disordered potential,  $\tilde{V}(x, y)$ , given by

$$V_m(x) \equiv \int_0^{L_y} \frac{dy}{L_y} e^{2\pi i m y/L_y} \tilde{V}(x, y). \quad (2)$$

LLL-projection suppresses non-zero wave vectors and gives  $t/v \sim e^{-\pi^2 \ell_B^2/L_y^2} \ll 1$ . Further-neighbor hopping terms in Eq. (1) are exponentially smaller than  $t$  and hence can be neglected. In the following, we take  $t_n \equiv t e^{i\theta_x/L_x}$  for simplicity, as the precise values are unimportant. The angles  $\theta$  assume very different roles in this limit:  $\theta_x$  is the magnetic flux through the ring, while  $\theta_y$  is the parameter of a Thouless pump [36] which smoothly moves the Landau orbits relative to the background potential. At any fixed  $\theta$ , the Hamiltonian of Eq. (1) is Anderson localized. As the pump parameter  $\theta_y$  is adiabatically taken through a cycle, the random on-site potentials  $v_n(\theta_y)$  change smoothly and the system undergoes spectral flow: at the end of the cycle,  $v_n(2\pi) = v_{n+1}(0)$ , so the initial and final spectra coincide up to a  $n \mapsto n+1$  translation. However, following each eigenstate through the adiabatic cycle reveals an interesting picture.

Adiabatically changing a local chemical potential in an Anderson insulator leads to non-local charge transport [39] due to avoided resonances between the site being

manipulated and arbitrarily distant ones (the distance is practically limited by  $\log \tau$ , where  $\tau$  is the time scale of the adiabatic manipulation, which we can take to be infinite for calculating  $C$ ). In the present setting, varying  $\theta_y$  adiabatically manipulates *all random fields at once*, giving rise to a complicated network of resonances and thus more intricate patterns of charge transfer across the system. However, as a consequence of adiabaticity, energy levels can never cross, so an electron that starts the cycle in orbital  $n$  ends in orbital  $n-1$  (i.e., at the same point in real space). Whenever an avoided crossing between sites  $n_1$  and  $n_2$  takes place, charge is transported through the shortest path [40]. One may expect each electron to take a local random walk in the vicinity of its initial site  $n_i$  and end the cycle at site  $n_i - 1$ . However, this cannot be the case for every electron: at least one must wind around the entire ring during the cycle. Indeed, if  $W_n$  is the winding number of the electron initially at site  $n$ , it can be shown with simple algebra [38] that  $\sum_n W_n = 1$ .

This bears intriguing similarity to the total Chern number of the Landau level,  $\sum_n C_n = 1$ . In fact, such an identification is correct: the Chern number  $C_n$  reduces to the winding number  $W_n$  in the thin-torus limit. This can be seen by considering the phase acquired during a loop around the “Brillouin zone” defined by  $\theta$ . Threading flux  $\theta_x$  does nothing to an Anderson localized wavefunction, whereas threading  $\theta_y$  across a cycle causes it to wind  $W_n$  times around the ring, which encircles the  $\theta_x$  flux. The phase acquired is thus  $e^{2\pi i W_n}$ , giving  $C_n = W_n$ . This can be straightforwardly made rigorous by partitioning the  $\theta$  torus into thin rectangular strips, so phases are defined unambiguously [38]. This identification is the key to explaining the observed proliferation of Chern states under 1D scaling. In essence, during a Thouless pump cycle, every electron hops randomly and non-locally across the chain many times, generically acquiring a large winding number, which translates to a large Chern number.

*Dimensional crossover.* Even though the thin-torus limit  $L_y \ll \ell_B$  is a helpful simplification, the physics described above remains valid for  $L_y > \ell_B$ , as long as  $a \gg 1$ . Hopping matrix elements are not negligible up to a real-space distance  $\mathcal{O}(\ell_B)$ , i.e. a number of sites  $\mathcal{O}(L_y/\ell_B)$ . These matrix elements are responsible for local level repulsion and strongly suppress energy fluctuations during the Thouless pump cycle. To get a quantitative measure of this, we start from a square torus. There, we know from numerical investigations that the average Thouless conductance obeys  $g(E, L) \simeq G(EL^{1/\nu_{2D}})$ , where  $G$  is a scaling function well approximated by a Gaussian,  $G(x) \sim g_0 e^{-x^2/2\sigma^2}$ , and  $g_0, \sigma$  are  $\mathcal{O}(1)$  constants. Inverting the definition of  $g$  yields an estimate of the energy fluctuations of a typical state during the pump cycle:

$$\delta E \sim \frac{2\pi v g_0}{L^2} \exp\left(-\frac{E^2}{2\sigma^2} L^{2/\nu_{2D}}\right). \quad (3)$$

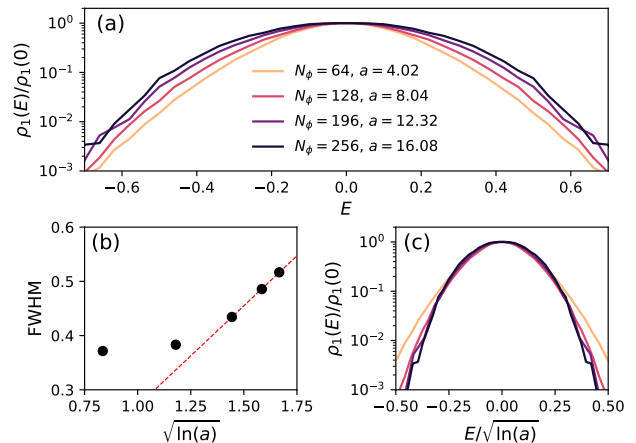


FIG. 2. (a) Density of  $C = 1$  states  $\rho_1(E)$  for  $L_y = 10\ell_B$  and different aspect ratios  $a$ . (b) Full width at half maximum of  $\rho_1$  indicates broadening consistent with Eq. (5). (c) Rescaling the energy by  $\sqrt{\ln(a)}$  collapses the curves for different sizes.

Here  $v$  is the bandwidth and  $2\pi v/L^2$  is the typical level spacing. As  $\delta E$  is determined by the range of local hopping matrix elements, Eq. (3) remains true if we consider a rectangular torus and replace  $L$  with the *short* circumference  $L_y$ . The expected number of avoided resonances encountered during a pump cycle,  $N_r$ , is simply the number of states in the spectrum with energies within the range of fluctuations  $\delta E$ . Approximating  $\rho(E) \simeq L_x L_y / 2\pi v$  yields

$$N_r \sim \rho(E) \delta E \sim g_0 \frac{L_x}{L_y} \exp\left(-\frac{E^2}{2\sigma^2} L_y^{2/\nu_{2D}}\right). \quad (4)$$

Thus, even away from the band center, and even for  $L_y > \ell_B$ , 1D scaling eventually makes  $a$  large enough that  $N_r \gtrsim 1$ . At that point the crossover between 2D and 1D behavior takes place, with typical states acquiring nontrivial winding and thus Chern number. This crossover happens unevenly in energy: it starts at the band center (where one already has Chern states even in the 2D thermodynamic limit) and spreads towards the band edges. The contour defining the dimensional crossover is approximately fixed by setting  $N_r = 1$ :

$$E \sim \sqrt{\ln(a)} \quad (5)$$

This prediction is borne out by numerical data on the density of Chern states,  $\rho_C(E)$ . Fig. 2 shows that the broadening of  $\rho_{\text{top}}$ , already visible in Fig. 1, is explained fairly accurately as a scaling collapse of  $\rho_1(E/\sqrt{\ln(a)})$ , for  $a$  large enough. While numerical instability prevents us from following the crossover to larger  $a$ , where all states are predicted to become topological, results are consistent with the above picture.

*Thouless conductance.* As mentioned earlier, while 1D scaling causes the proliferation of Chern states across the

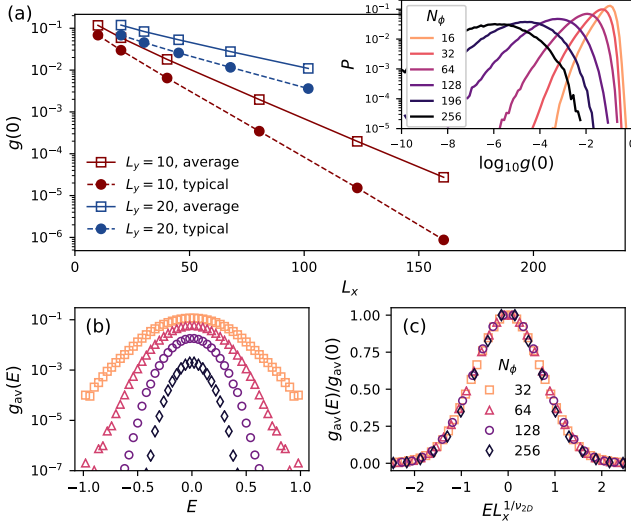


FIG. 3. (a) Average and typical values of the Thouless conductance at the center of the band,  $g(0)$ , for fixed  $L_y$ , as a function of  $L_x$ . Inset: the distribution of  $\log_{10} g(0)$  for  $L_y = 10\ell_B$ , increasing  $N_\phi$ . (b) The average Thouless conductance  $g_{av}(E)$  for  $L_y = 14\ell_B$  decays with increasing  $N_\phi$ . (c) The normalized quantity  $g_{av}(E)/g_{av}(0)$  shows scaling collapse under  $E \mapsto EL_x^{1/\nu_{2D}}$  with critical exponent  $\nu_{2D} \simeq 2.4$ .

spectrum, it also removes the critical energy characteristic of the 2D problem and makes the entire spectrum Anderson-localized. We verify this numerically by calculating the disorder- and eigenstate-averaged Thouless conductance  $g_{av}(E)$ , Fig. 3. Unlike the 2D case, where at the center of the band  $g_{av}(0) \sim \mathcal{O}(1)$  as  $L \rightarrow \infty$ , here it decays exponentially in  $L_x$ ,  $g_{av}(0) \sim e^{-L_x/\xi_1}$ , with  $\xi_1 \simeq 1.7L_y$ , as expected for a 1D problem. However, surprisingly, the normalized quantity  $\tilde{g}_{av}(E) \equiv g_{av}(E)/g_{av}(0)$  displays scaling collapse with the *same* critical exponent as the two-dimensional case,  $\nu_{2D} \sim 2.4$  [41]. These results seem contradictory: on the one hand, a finite  $\xi_1$  suggests localization across the spectrum with no critical energy; nevertheless, we observe signatures of a divergent  $\xi_2 \sim E^{-\nu_{2D}}$ , reproducing the 2D critical behavior, even as the scaling is purely one-dimensional.

The variation of  $g$  across samples and eigenstates sheds light on this issue. At the center of the band, the distribution of  $\ln(g)$  broadens as  $L_x$  is increased, so that the typical value  $g_{typ} \equiv e^{\langle \ln g \rangle}$  decays exponentially faster than the average value  $g_{av}$ . In the thermodynamic limit, the peak in  $g_{av}(E)$  near  $E = 0$  is thus dominated by rare states that are abnormally extended in the *long* direction ( $\hat{x}$ ). We attribute the appearance of  $\nu_{2D}$  to these atypical states: states percolating across the sample in  $L_x$  but not in  $L_y$  are by construction unaware of the aspect ratio, and thus display the 2D critical behavior as  $L_x$  is increased. As  $L_x$  grows, these states become exponentially rare, which explains the vanishing amplitude of

the signal and its presence in  $g_{av}$  but not  $g_{typ}$ .

*Discussion.* We have investigated the fate of the quantum Hall plateau transition when finite-size scaling is performed for one of the two dimensions only. Through numerical diagonalization, we have uncovered surprising and counter-intuitive behavior: Anderson localization across the spectrum, accompanied by the proliferation of Chern states. This led us to investigate the fate of the Chern number, a two-dimensional topological invariant, in the quasi-one-dimensional limit defined by  $a = L_x/L_y \gg 1$ . In the thin-torus limit  $L_y \ll \ell_B$ , the system maps onto a 1D fermionic chain and the flux through the short loop of the torus becomes a Thouless pump parameter that smoothly shifts the random chemical potentials of the fermion chain. We have shown that in this limit the Chern number  $C$  of a wavefunction maps onto the winding number  $W$  of the electron around the system (now a one-dimensional ring) over the course of a pump cycle, which is determined by a random network of avoided crossings in the spectrum of the system. This identification consistently gives the total Chern number of the band and leads to some striking predictions, e.g. that generic states in this limit have large, random Chern number, and that percolating in either direction may allow states to acquire a non-zero Chern number.

We have further shown that this picture is valid away from the thin-torus limit, i.e. for  $L_y > \ell_B$ , as long as the torus aspect ratio  $a$  is large enough. The crossover between 2D and 1D behavior as  $a$  is increased occurs unevenly in energy: it starts at the band center and spreads towards the band edges. The broadening is predicted to be very slow,  $\sim \sqrt{\ln(a)}$ , but it is nonetheless visible in our numerics at  $L_y/\ell_B \sim \mathcal{O}(10)$ , quite far from the thin-torus limit.

On a theoretical level, our findings provide an example of subtle interplay of topology and disorder. The idea of topological pumping, which goes back to Thouless [36], is a subject of rising theoretical interest, especially in connection to Floquet physics [42–44] or synthetic dimensions [45]. Here it is applied in a new context, in the presence of disorder, and provides the key to interpret the quasi-1D limit of the quantum Hall plateau transition.

We conclude with some remarks related to experiment. As the non-local avoided crossings that underpin the picture presented here are generally very narrow (exponentially in system size), the adiabatic time scales required to observe this behavior in macroscopic systems are unphysically long. However, for microscopic systems, the manipulations required may still be performed adiabatically. The ingredients required are (i) adiabatically tunable, pseudo-random on-site chemical potentials, (ii) nearest-neighbor hopping, and (iii) sufficiently long coherence times (relative to the required adiabatic time scale). Clean Thouless pumps have been successfully engineered using ultracold bosonic [46, 47] or fermionic [48] atoms in optical superlattices, single

spins in diamond [49], Bose-Einstein condensates [50] and quantum dots [51, 52]. Finally, while periodic boundary conditions are required to observe the winding, the striking coexistence of Anderson localization and non-local charge transport across the length of the system would be present and observable even with open boundary conditions.

This work was supported by DOE BES grant DE-SC0002140. We acknowledge useful conversations with Shivaji Sondhi.

- 
- [1] K. v. Klitzing, G. Dorda, and M. Pepper, *Phys. Rev. Lett.* **45**, 494 (1980).
  - [2] R. B. Laughlin, *Phys. Rev. B* **23**, 5632 (1981).
  - [3] D. J. Thouless, M. Kohmoto, M. P. Nightingale, and M. den Nijs, *Phys. Rev. Lett.* **49**, 405 (1982).
  - [4] R. E. Prange, *Phys. Rev. B* **23**, 4802 (1981).
  - [5] B. Huckestein, *Rev. Mod. Phys.* **67**, 357 (1995), and references therein.
  - [6] H. P. Wei, D. C. Tsui, M. A. Paalanen, and A. M. M. Pruisken, *Phys. Rev. Lett.* **61**, 1294 (1988).
  - [7] L. W. Engel, D. Shahar, C. Kurdak, and D. C. Tsui, *Phys. Rev. Lett.* **71**, 2638 (1993).
  - [8] W. Li, C. L. Vicente, J. S. Xia, W. Pan, D. C. Tsui, L. N. Pfeiffer, and K. W. West, *Phys. Rev. Lett.* **102**, 216801 (2009).
  - [9] S. Kivelson, D.-H. Lee, and S.-C. Zhang, *Phys. Rev. B* **46**, 2223 (1992).
  - [10] I. A. Gruzberg, A. Klümper, W. Nuding, and A. Sedrakyan, *Phys. Rev. B* **95**, 125414 (2017).
  - [11] Q. Zhu, P. Wu, R. N. Bhatt, and X. Wan, *Phys. Rev. B* **99**, 024205 (2019).
  - [12] M. Puschmann, P. Cain, M. Schreiber, and T. Vojta, *Phys. Rev. B* **99**, 121301 (2019).
  - [13] B. Huckestein and B. Kramer, *Phys. Rev. Lett.* **64**, 1437 (1990).
  - [14] B. Huckestein, *Europhysics Letters (EPL)* **20**, 451 (1992).
  - [15] J. T. Chalker and P. D. Coddington, *Journal of Physics C: Solid State Physics* **21**, 2665 (1988).
  - [16] D.-H. Lee, Z. Wang, and S. Kivelson, *Phys. Rev. Lett.* **70**, 4130 (1993).
  - [17] K. Slevin and T. Ohtsuki, *Phys. Rev. B* **80**, 041304 (2009).
  - [18] H. Obuse, I. A. Gruzberg, and F. Evers, *Phys. Rev. Lett.* **109**, 206804 (2012).
  - [19] Y. Huo and R. N. Bhatt, *Phys. Rev. Lett.* **68**, 1375 (1992).
  - [20] D. P. Arovas, R. N. Bhatt, F. D. M. Haldane, P. B. Littlewood, and R. Rammal, *Phys. Rev. Lett.* **60**, 619 (1988).
  - [21] K. Yang and R. N. Bhatt, *Phys. Rev. Lett.* **76**, 1316 (1996).
  - [22] K. Yang and R. N. Bhatt, *Phys. Rev. B* **55**, R1922 (1997).
  - [23] K. Yang and R. N. Bhatt, *Phys. Rev. B* **59**, 8144 (1999).
  - [24] D. N. Sheng and Z. Y. Weng, *Phys. Rev. Lett.* **75**, 2388 (1995).
  - [25] D. N. Sheng and Z. Y. Weng, *Phys. Rev. Lett.* **78**, 318 (1997).
  - [26] D. N. Sheng, X. Wan, E. H. Rezayi, K. Yang, R. N. Bhatt, and F. D. M. Haldane, *Phys. Rev. Lett.* **90**, 256802 (2003).
  - [27] X. Wan, D. N. Sheng, E. H. Rezayi, K. Yang, R. N. Bhatt, and F. D. M. Haldane, *Phys. Rev. B* **72**, 075325 (2005).
  - [28] R. N. Bhatt, in *Physical Phenomena at High Magnetic Fields, Proceedings of the National High Magnetic Field Laboratory Conference, Tallahassee, Florida*, edited by E. Manousakis (Addison-Wesley, Reading, 1992) p. 65.
  - [29] M. Ippoliti, S. D. Geraedts, and R. N. Bhatt, *Phys. Rev. B* **97**, 014205 (2018).
  - [30] J. Priest, S. P. Lim, and D. N. Sheng, *Phys. Rev. B* **89**, 165422 (2014).
  - [31] X. Wang, Q. Li, and C. M. Soukoulis, *Phys. Rev. B* **58**, 3576 (1998).
  - [32] N. Sandler, H. R. Maei, and J. Kondev, *Phys. Rev. B* **70**, 045309 (2004).
  - [33] D. Thouless, *Physics Reports* **13**, 93 (1974).
  - [34] S. Kettmann, *Phys. Rev. B* **69**, 035339 (2004).
  - [35] A. Struck, B. Kramer, T. Ohtsuki, and S. Kettmann, *Phys. Rev. B* **72**, 035339 (2005).
  - [36] D. J. Thouless, *Phys. Rev. B* **27**, 6083 (1983).
  - [37] T. Fukui, Y. Hatsugai, and H. Suzuki, *Journal of the Physical Society of Japan* **74**, 1674 (2005).
  - [38] See Online Supplemental Material for details on the numerical calculations, a proof of the identity between Chern number and winding number during a Thouless pump cycle, and additional data on the density of Chern states.
  - [39] V. Khemani, R. Nandkishore, and S. L. Sondhi, *Nature Physics* **11**, 560 (2015).
  - [40] The perturbative hopping amplitude for a path of length  $d$  is  $\sim (t/v)^d$  so the shortest path is exponentially favored. Randomness in  $v_n$  may only change this conclusion if the two paths have similar lengths, which is rare in the thermodynamic limit, or if  $v_n = 0$  occurs with finite probability, which requires a singular distribution  $P(v)$ .
  - [41] Such collapse is not seen for typical  $g$ .
  - [42] I. Martin, G. Refael, and B. Halperin, *Phys. Rev. X* **7**, 041008 (2017).
  - [43] P. Weinberg, M. Bukov, L. D'Alessio, A. Polkovnikov, S. Vajna, and M. Kolodrubetz, *Physics Reports* **688**, 1 (2017).
  - [44] M. H. Kolodrubetz, F. Nathan, S. Gazit, T. Morimoto, and J. E. Moore, *Phys. Rev. Lett.* **120**, 150601 (2018).
  - [45] I. Petrides, H. M. Price, and O. Zilberberg, *Phys. Rev. B* **98**, 125431 (2018).
  - [46] M. Lohse, C. Schweizer, O. Zilberberg, M. Aidelsburger, and I. Bloch, *Nature Physics* **12**, 350 (2015).
  - [47] M. Lohse, C. Schweizer, H. M. Price, O. Zilberberg, and I. Bloch, *Nature* **553**, 55 (2018).
  - [48] S. Nakajima, T. Tomita, S. Taie, T. Ichinose, H. Ozawa, L. Wang, M. Troyer, and Y. Takahashi, *Nature Physics* **12**, 296 (2016).
  - [49] W. Ma, L. Zhou, Q. Zhang, M. Li, C. Cheng, J. Geng, X. Rong, F. Shi, J. Gong, and J. Du, *Phys. Rev. Lett.* **120**, 120501 (2018).
  - [50] H.-I. Lu, M. Schemmer, L. M. Ayccock, D. Genkina, S. Sugawa, and I. B. Spielman, *Phys. Rev. Lett.* **116**, 200402 (2016).
  - [51] M. Switkes, C. M. Marcus, K. Campman, and A. C. Gossard, *Science* **283**, 1905 (1999).
  - [52] M. R. Buitelaar, V. Kashcheyevs, P. J. Leek, V. I. Talyanskii, C. G. Smith, D. Anderson, G. A. C. Jones, J. Wei,

and D. H. Cobden, [Phys. Rev. Lett. \*\*101\*\*, 126803 \(2008\)](#).

# Supplemental Material: Dimensional crossover of the integer quantum Hall plateau transition and disordered topological pumping

Matteo Ippoliti<sup>1</sup> and R. N. Bhatt<sup>2</sup>

<sup>1</sup>Department of Physics and <sup>2</sup>Department of Electrical Engineering, Princeton University, Princeton, NJ 08544

## DETAILS OF NUMERICAL CALCULATION

We consider a continuum model of electrons in a high magnetic field projected into the LLL. The system is set on a rectangular torus with sides  $L_x$ ,  $L_y$  and generalized periodic boundary conditions parametrized by angles  $\boldsymbol{\theta} \equiv (\theta_x, \theta_y) \in [0, 2\pi)^2$ . The torus is pierced by  $N_\phi$  quanta of magnetic flux, i.e.  $L_x L_y = 2\pi N_\phi$ . The wavefunctions in Landau gauge are given by

$$\psi_n(x, y) = \frac{1}{\sqrt{L_y \pi^{1/2}}} \sum_{p \in \mathbb{Z}} e^{ip\theta_x} e^{ik_{n,p}(\theta_y)y - \frac{1}{2}(x - k_{n,p}(\theta_y))^2} \quad (\text{S1})$$

with  $k_{n,p}(\theta_y) = 2\pi(n + pN_\phi + \theta_y/2\pi)/L_y$ .

Disorder is represented by a Gaussian white noise potential  $V_{\mathbf{q}}$  obeying

$$\langle V_{\mathbf{q}_1} V_{\mathbf{q}_2} \rangle = V_0^2 \delta^2(\mathbf{q}_1 + \mathbf{q}_2). \quad (\text{S2})$$

A straightforward calculation yields the Hamiltonian matrix elements in the basis of Eq. (S1):

$$\begin{aligned} H_{n_1, n_2} &= \sum_{p, m_x, m_y \in \mathbb{Z}} e^{ip\theta_x} \delta(n_2 - n_1 + pN_\phi = m_y) \tilde{V}_{\mathbf{q}} \\ &\times e^{-2\pi i(n_1 + m_y/2 + \theta_y/2\pi)m_x/N_\phi} \end{aligned} \quad (\text{S3})$$

where  $\tilde{V}_{\mathbf{q}} \equiv V_{\mathbf{q}} e^{-\frac{1}{4}q^2}$  is the LLL-projected potential, and  $\mathbf{q} = 2\pi(m_x/L_x, m_y/L_y)$ .

In order to calculate the Chern number of each eigenstate in the spectrum of  $H$  from Eq. (S3), we follow the standard method described in Ref. [37] and split the torus of boundary angles  $\boldsymbol{\theta}$  into a lattice,  $\boldsymbol{\theta}_{i,j} = 2\pi(i/N_x, j/N_y)$ . Appropriate values of the mesh size were discussed in Ref. [11], which takes  $N_x = N_y = \sqrt{4\pi N_\phi/3}$ . Unlike the present work, Ref. [11] only deals with square systems where  $N_x = N_y$  is clearly optimal. We fix the product to the same value,  $N_x N_y \gtrsim 4\pi N_\phi/3$ , but we find that a rectangular mesh with  $N_x/N_y \simeq L_y/L_x$  is optimal. This is physically reasonable as the angle in the *short* direction affects the *long* boundary, and *vice versa*.

For each site on this lattice, we diagonalize Eq. (S3) numerically and obtain the spectrum  $\{|\theta_{ij}, n\rangle, n = 0, \dots, N_\phi - 1\}$ . We then assign a  $U(1)$  gauge variable to each bond in the lattice:

$$A_n^x(i, j) \equiv \frac{\langle \boldsymbol{\theta}_{ij}, n | \boldsymbol{\theta}_{i+1, j}, n \rangle}{|\langle \boldsymbol{\theta}_{ij}, n | \boldsymbol{\theta}_{i+1, j}, n \rangle|}, \quad A_n^y(i, j) \equiv \frac{\langle \boldsymbol{\theta}_{ij}, n | \boldsymbol{\theta}_{i, j+1}, n \rangle}{|\langle \boldsymbol{\theta}_{ij}, n | \boldsymbol{\theta}_{i, j+1}, n \rangle|} \quad (\text{S4})$$

for horizontal and vertical bonds, respectively. The curvature of this gauge field is given by the “integral” around a plaquette:

$$U_n(i, j) \equiv A_n^x(i, j) A_n^y(i+1, j) A_n^x(i, j+1)^* A_n^y(i, j)^*.$$

If the mesh is fine enough (i.e.  $N_x, N_y$  are large enough),  $|U_n(i, j) - 1| \ll 1$  and one can define  $\gamma_n(i, j) \equiv \ln U_n(i, j)$  without ambiguity in the choice of branch cut for the logarithm. The Chern number is then

$$C_n \equiv \frac{1}{2\pi i} \sum_{i, j} \gamma_n(i, j). \quad (\text{S5})$$

This method also gives us access to all the energies  $E_n(i, j)$ , which we use to compute the Thouless conductance.

A subtlety implicit in formulae Eq. (S4) is that the inner products involve wavefunctions with different boundary conditions. The matrices implementing such inner products are not equal to the identity and must be calculated. As we sample  $\boldsymbol{\theta}$  from a rectangular lattice and only need inner products between neighboring points in that lattice, we are interested in

$$\mathcal{N}_{mn}(\boldsymbol{\theta}; \boldsymbol{\theta} + \mu \hat{j}) \equiv \langle \psi_m(\boldsymbol{\theta}) | \psi_n(\boldsymbol{\theta} + \mu \hat{j}) \rangle \quad (\text{S6})$$

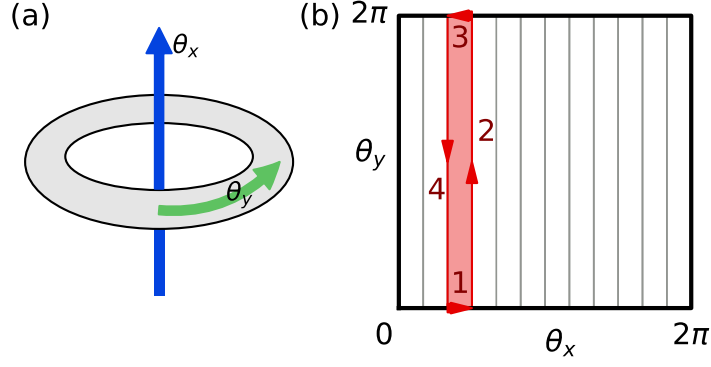


FIG. S1. (a) Sketch of a thin torus system. The two boundary angles correspond to fluxes through the long ( $\theta_x$ ) and short ( $\theta_y$ ) non-trivial loops of the torus, respectively. (b) The partitioning of the  $\theta$  torus used to calculate the Chern number. All slices contribute the same amount. The sides of the highlighted slice are numbered according to the discussion in the text.

for  $\hat{j} = \hat{x}, \hat{y}$ .

For  $\hat{j} = \hat{y}$ , we have

$$\begin{aligned} \mathcal{N}_{mn}(\theta, \theta + \mu \hat{y}) &= \frac{1}{L_y \sqrt{\pi}} \sum_{P, p \in \mathbb{Z}} e^{ip\theta_x} \int dy e^{ik_{n-m,p}(\mu)y} \int_{PL_x}^{(P+1)L_x} dx \exp \left[ - \left( x - k_{\frac{n+m}{2}, \frac{p}{2}}(\theta_y + \mu/2) \right)^2 - \frac{1}{4} k_{n-m,p}^2(\mu) \right] \\ &= \sum_{p \in \mathbb{Z}} e^{ip\theta_x} \frac{e^{ik_{n-m,p}(\mu)L_y} - 1}{ik_{n-m,p}(\mu)L_y} e^{-\frac{1}{4} k_{n-m,p}^2(\mu)}, \end{aligned} \quad (\text{S7})$$

where  $k_{n,p}(\mu) = \frac{2\pi}{L_y}(n + N_\phi p + \mu/2\pi)$ . One can verify that this reduces to the identity for  $\mu \rightarrow 0$ . Moreover the entries only depend on the difference  $n - m$ . For  $\hat{j} = \hat{x}$ , we have instead

$$\begin{aligned} \mathcal{N}_{mn}(\theta, \theta + \mu \hat{x}) &= \frac{1}{L_y \sqrt{\pi}} \sum_{P, p \in \mathbb{Z}} e^{ip\theta_x + i(p+P)\mu} \int dy e^{ik_{n-m,p}(0)y} \int_0^{L_x} dx \exp \left[ - \left( x - k_{\frac{n+m}{2}, P+\frac{p}{2}}(\theta_y) \right)^2 - \frac{1}{4} k_{n-m,p}^2(0) \right] \\ &= \delta_{mn} \frac{1}{\sqrt{\pi}} \sum_{P \in \mathbb{Z}} e^{iP\mu} \int_{PL_x}^{(P+1)L_x} dx e^{-(x - k_{n,0}(\theta_y))^2}, \end{aligned} \quad (\text{S8})$$

where we used the fact that the  $y$  integral gives a  $\delta$  function to arrive to the result. This matrix is diagonal and reduces to the identity for  $\mu \rightarrow 0$  as well. Moreover, we verify numerically that for  $L_x = L_y$  the two matrices are conjugate to each other. This reflects the fact that the two must map into each other under a  $\pi/2$  rotation followed by a gauge transformation.

## PROOF OF THE IDENTITY BETWEEN CHERN NUMBER AND WINDING NUMBER

We calculate the Chern number by splitting the “Brillouin zone”  $\theta \in [0, 2\pi)^2$  in many vertical strips,  $\theta_y \in [0, 2\pi)$ ,  $\theta_x \in [m\varepsilon, (m+1)\varepsilon)$ , for  $\varepsilon = 2\pi/M \ll 1$ ,  $m, M \in \mathbb{Z}$ , as sketched in Fig. S1. Similarly to the numerical approach, we calculate the phase for transporting the wavefunction around each side of each small rectangle, then add all the contributions. The cycle goes as follows:

1. Increase  $\theta_x$  from  $m\varepsilon$  to  $(m+1)\varepsilon$  at fixed  $\theta_y$ . This twist of boundary conditions has no effect on a perfectly Anderson-localized orbital.
2. Increase  $\theta_y$  from 0 to  $2\pi$  at fixed  $\theta_x$ . During this step, the electron winds  $W_i$  times around the circle and acquires an Aharonov-Bohm phase  $e^{i\theta_y W_i} = e^{i(m+1)\varepsilon W_i}$ , where  $\theta_y = (m+1)\varepsilon$  is the flux through the circle. An example is sketched in Fig. S2
3. Decrease  $\theta_x$  from  $(m+1)\varepsilon$  to  $m\varepsilon$ . Like step 1, this has no effect.

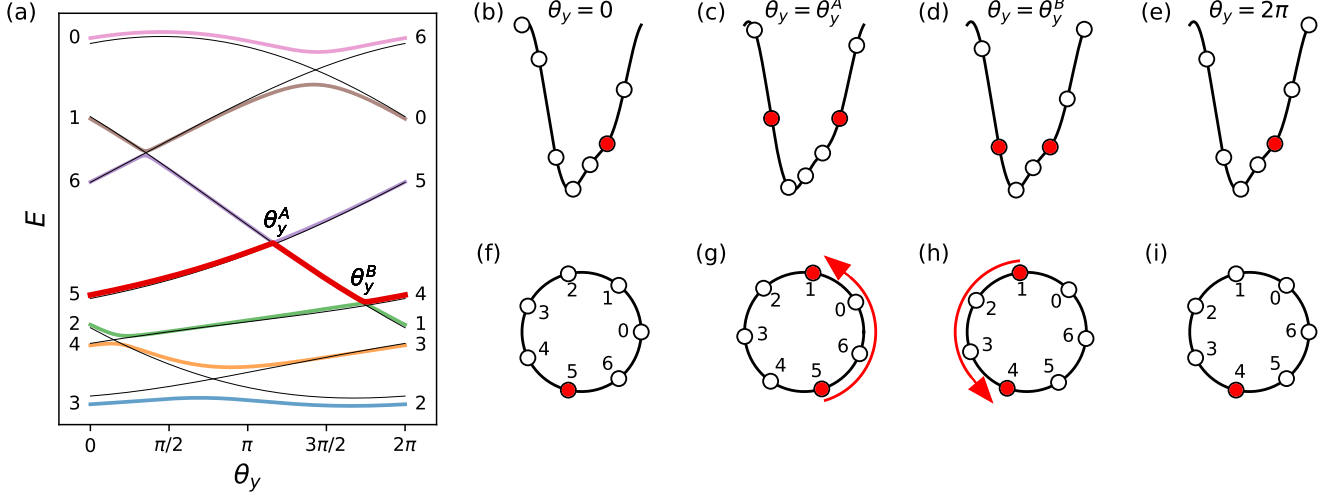


FIG. S2. (a) Energy levels (thick lines) and on-site chemical potentials (thin lines) as a function of Thouless pump parameter  $\theta_y$  for a simple example with  $N = 7$  orbitals. All states have  $C = 0$  except the one starting at orbital 5. (b-e) Evolution of the chemical potentials at four points during the cycle,  $\theta_y = 0, \theta_y^A, \theta_y^B, 2\pi$ . White circles denote empty orbitals, red circles occupied orbitals. At  $\theta_y^{A,B}$  the occupied orbital is at resonance with an empty orbital, an avoided crossing opens, and the electron hops. (f-i) View of the same cycle in real space, showing how the electron's path winds once around the system during each cycle.

4. Decrease  $\theta_y$  from  $2\pi$  to 0. The electron winds  $-W_i$  times around the circle (as the evolution is perfectly reversible) and acquires a phase  $e^{-iW_i m \varepsilon}$ , completing the cycle.

The net phase acquired by the electron wavefunction is  $U_m = e^{iW_i \varepsilon}$ . Since  $\varepsilon \ll 1$ , one can take the logarithm unambiguously and obtain the Chern number:

$$C_i = \frac{1}{2\pi i} \sum_{m=1}^M \ln U_m = W_i. \quad (\text{S9})$$

This derivation relies on a few assumptions, namely that (i) the electron orbital is Anderson-localized at every  $\theta_x = m\varepsilon$ , and (ii)  $W_i$  does not depend on  $\theta_x$ . The first assumption is satisfied in the thin-torus limit. The electron typically resonates between orbitals at a distance  $\sim \mathcal{O}(N_\phi)$ , so the gap at the avoided crossing is  $\sim (t/v)^{N_\phi}$ . Therefore the fraction of the interval  $\theta_x \in [0, 2\pi)$  spent in a non-local superposition is exponentially small in system size and asymptotically has measure 0. That  $W_i$  doesn't depend on  $\theta_x$  in this limit follows from similar considerations.

A natural consistency check on the identification of Chern number and winding number is that one should always have  $\sum_i W_i = 1$ , so as to match the total Chern number of the Landau level. Avoided crossings (absent fine-tuning) happen at isolated points in the  $\theta_x$  interval and involve only a pair of states each. Therefore, the question can be rephrased as a simple combinatorial problem: showing that any decomposition of the cyclic permutation  $\mathcal{C} : (1, 2, \dots, N) \mapsto (2, 3, \dots, N, 1)$  (representing the spectral flow) as a product of pairwise swaps  $\mathcal{S}_{ij}$  (representing the avoided crossings) gives a total winding number of 1.

This can be shown as follows. Let one such decomposition be  $\mathcal{C} = \prod_c \mathcal{S}_{n_1(c), n_2(c)}$ . Define a matrix of integers  $d_{c,i}$  as the distance element  $i$  traverses during move  $c$ , with sign (this is 0 for all elements except the two being swapped,  $i = n_{1,2}(c)$ , which have opposite values). By this definition, the sum of each row is trivially  $\sum_i d_{c,i} = 0$ . The sum of each column  $i$  is the total distance traversed by element  $i$ , which must be  $-1 \pmod N$ ; we set  $\sum_c d_{c,i} = NW_i - 1$ , defining the winding number  $W_i$ . Putting the two together, we get

$$\sum_{c,i} d_{c,i} = N \left( -1 + \sum_i W_i \right) = 0 \quad (\text{S10})$$

hence  $\sum_i W_i = 1$ . In a Chern- $k$  band, one would have to replace  $\mathcal{C}$  with  $\mathcal{C}^k$  (as the spectral flow cycles the orbitals  $k$  times in a Chern- $k$  band) and correctly obtain  $\sum_i W_i = k$ .

### ADDITIONAL DATA ON DENSITY OF CHERN STATES

Here we report additional data on the density of states  $\rho_C(E)$  parsed by Chern number  $C$  beyond what is shown in Fig. 1 in the main text. We consider rectangular tori with  $L_x = 10\ell_B$  (Fig. S3) and  $L_x = 20\ell_B$  (Fig. S4) and scale  $L_y$ . Doing so causes both a broadening of  $\rho_{\pm 1}$  and an increase in the density of higher- $|C|$  states. Comparing the two  $L_x$  values shows how this behavior is due to the 2D-1D crossover controlled by the aspect ratio  $a = L_y/L_x$ , as opposed to 2D behavior controlled solely by the system size  $N_\phi$ .

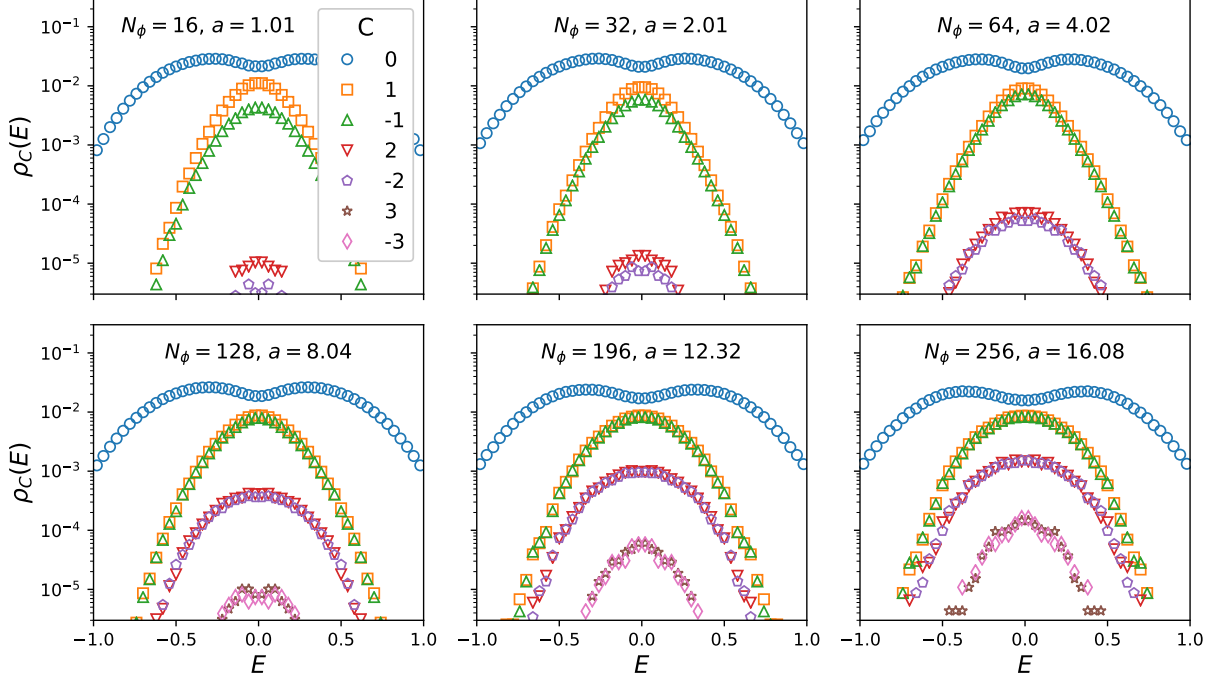


FIG. S3. Density of states with Chern number  $C$ ,  $\rho_C(E)$ , for rectangular tori with  $L_x = 10\ell_B$  and variable  $N_\phi$  indicated on each panel. As  $N_\phi$  increases the system gradually approaches the 1D regime: more and more states become topological ( $C \neq 0$ ), due both to the broadening of  $\rho_{\pm 1}(E)$  and to states with higher  $|C|$  becoming more common at the band center.

While the density of Chern- $C$  states broadens for each  $C$ , the linear combination  $\sum_C C\rho_C$  remains constant, as seen by looking at the disorder-averaged Hall conductance,

$$\sigma_{xy}(E) = \int_{-\infty}^E d\varepsilon \sum_{C \in \mathbb{Z}} C\rho_C(E), \quad (\text{S11})$$

shown in Fig. S5. Under 2D scaling,  $\sigma_{xy}(E)$  is known to collapse onto  $F(EL^{1/\nu_{2D}})$ , with  $F$  a scaling function. We conclude that the width of the crossover interval between the two conductance plateaus is fixed by the smallest side of the torus.

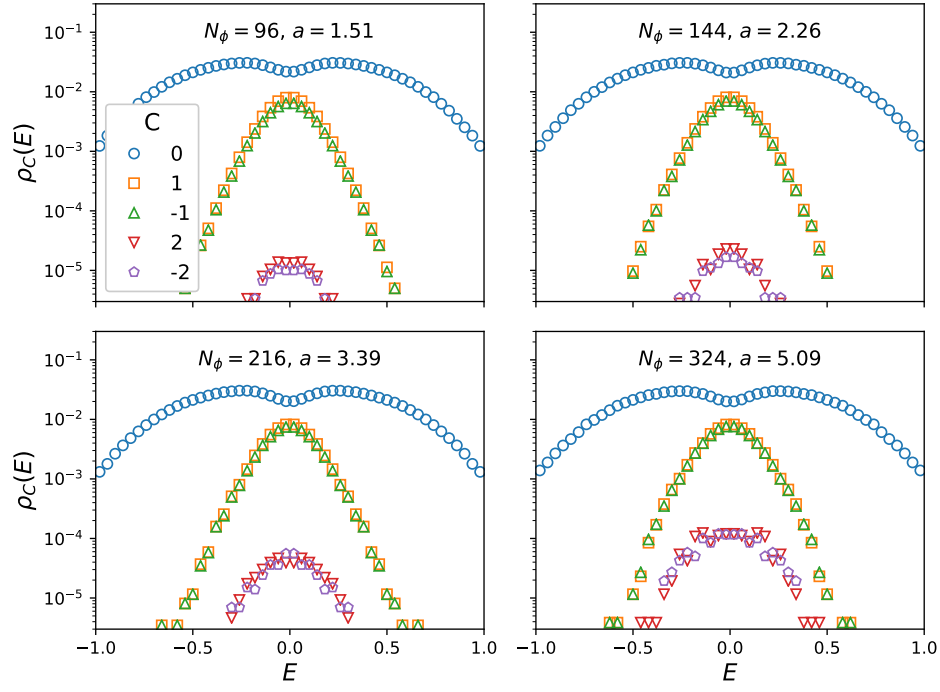


FIG. S4. Same as Fig. S3, but for  $L_x = 20\ell_B$  instead of  $10\ell_B$ . Despite the larger system size  $N_\phi$ , the aspect ratio we can achieve is smaller and the system is further away from the 1D limit:  $C = \pm 3$  states are still uncommon (below the displayed range) and the broadening of  $\rho_{\pm 1}$  is not as clear. Nonetheless the growth of  $C = \pm 2$  states is visible.

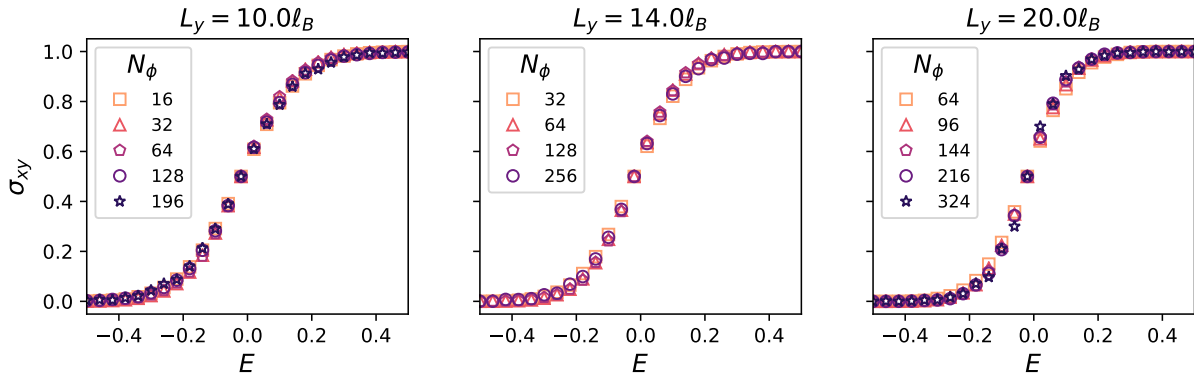


FIG. S5. Disorder-averaged Hall conductance  $\sigma_{xy}$  calculated from the densities  $\rho_C$  as in Eq. (S11).